Supporting Information

Simultaneously improving the delocalization of π electrons and directional transfer of charge carriers in carbon nitride for superior photocatalytic hydrogen evolution

Yujie Liang [a,#], Chi Cao [c,#], Lei Zeng [b,*], Haonan Wang [d,*], Yabin Jiang[a,*]

[a] Precision Medicine Laboratory for Chronic Non-communicable Diseases of Shandong Province, Institute of Precision Medicine, Jining Medical University, Jining, 272067, P. R. China

[b] School of Chemical Engineering and Pharmacy, Hubei Key Lab of Novel Reactor & Green Chemical Technology, Key Laboratory of Green Chemical Engineering Process of Ministry of Education, Wuhan Institute of Technology, No.206 Guanggu Road, East Lake New Technology Development Zone, Wuhan, 430072, P. R. China.

[c] State Key Laboratory of Inorganic Synthesis and Preparative Chemistry, College of Chemistry, Jilin University, Changchun 130012, P. R. China.

[d] School of Materials Science and Engineering, Changchun University, Changchun 130022, P. R. China

# These authors contributed equally to this work.

Corresponding Author
*E-mail: zl0613341@sina.com; wanghn@ccu.edu.cn; jiang01357@163.com

Experimental section

Synthesis of catalysts.

Synthesis of PCN and PCN-2AA-X. Typically, 10 g of urea and a certain amount of 2-Aminoterephthalic Acid (2AA) were mixed evenly in a mortar and ground for 15 minutes. The mixture was then calcined in a covered ceramic crucible at 550 °C for 2h with a heating rate of 5 °C·min^{-1}. The synthesized samples were denoted as PCN-2AA-X (X=0.5, 1, 3 and 5), in which X indicates the mass of the added 2AA. The pristine PCN sample was synthesized by a similar procedure, except that 2AA was not added. The fabrication process and possible structure of PCN-2AA photocatalyst are shown in Scheme 1.

Characterization of the Photocatalyst.

Scanning electron microscope (SEM) images and transmission electron microscope (TEM) images were observed by Zeiss Merlin field emission Scanning electron microscope (FESEM) and FEI Tecnai F30 Microscope TEM, respectively. The elemental composition of the samples was analyzed using energy dispersive X-ray (EDX) spectroscopy attached to the FESEM instrument. The crystal phases of the samples were analyzed using a Bruker D2 Phase X-Ray Diffractometer (Ni-filtered Cu Kα radiation, λ = 1.5406 Å). Fourier transform infrared (FT-IR) spectra were tested on a FT-IR spectrophotometer (Bruker VERTEX 70, 4000-500 cm-1). ^{13}C solid-state cross-polarized magic-angle spin nuclear magnetic resonance (MAS NMR) spectra were measured using a Bruker Advance 600 spectrometer. The elemental composition of the samples was analyzed by Kratos XSAM800 x-ray photoelectron spectroscopy (XPS), and the reference peak of its C1s was 284.8 eV. The samples were tested for elemental analysis (EA) on an Elementar Analysensysteme vario EL CUBE instrument. The N$_2$ adsorption isotherms of the samples were tested using an ASAP2020M device. The samples were first degassed at 300 °C for 6 hours under vacuum conditions, and then tested for nitrogen adsorption and desorption under liquid nitrogen (about -196°C). Electron paramagnetic spectra (EPR) were analyzed using a Bruker ESR JESFA200 spectrometer. The Ultraviolet and visible (UV-Vis) absorption spectra of the samples

were tested using UV-Vis absorption spectroscopy equipped with an integrating sphere. Photoluminescence (PL) and time-resolved photoluminescence (TR-PL) spectra of the samples were tested using Edinburgh Analytical Instruments FSTCSPC920 at room temperature.

Photoelectrochemical measurement

The CHI 660C electrochemical workstation (Chenhua, Shanghai) was carried out using a three-electrode system, in which the Ag/AgCl electrode was used as the reference electrode, the Pt wire was used as the counter electrode, and the aqueous solution of 0.1 M Na_2SO_4 was used as the electrolyte, coated with a small amount of photocatalyst. The glassy carbon electrode of the suspension is the working electrode. Moreover, the potentials in this work were all converted to reversible hydrogen electrode (RHE, $E_{RHE} = E_{Ag/AgCl} + 0.1987 + 0.05916pH$). At the same time, a 10 W LED lamp was used as the light source. Use this system to test transient photocurrent responses, electrochemical impedance spectroscopy (EIS) and Mott-Schottky plot.

Density-functional-theory (DFT) Calculations

To investigate the electronic structures and properties, we performed density functional theory (DFT) calculations using the Cambridge Sequential Total Energy Package (CASTEP). The Perdew-Burke-Ernzerhof (PBE) generalized gradient approximation (GGA) was employed to describe the exchange correlation functional. The cubic lattice two-dimensional melon sheet with lattice constants A = 16.7 Å and b = 12.4 Å is constructed as the basic model. The optimized molecular structure, band structure, density of states and hydrogen adsorption energy were simulated and calculated using the Vienna simulation package. At the same time, the exchange-correlation function approximated by PBE-type generalized gradient is used, and the gradient algorithm is optimized at the same time (force tolerance of 0.01 eV Å-1, kinetic energy cutoff of 500ev). The unit cell uses a $3 \times 4 \times 1$ k-point mesh in the 2D Brillouin zone.

Photocatalytic H_2 evolution

The activities of different photocatalysts were evaluated using a closed reactor (PerfectLight, Beijing). The photocatalytic hydrogen production performance of the

catalyst was tested by adding 10mg catalyst to 9mL water and 1mL triethanolamine mixed solution (containing 3 wt% $H_2PtCl_6 \cdot 6H_2O$). Before the reactions, the solution needs to be sonicated for 5 min. Next, the system was continuously stirred and irradiated, followed by testing the hydrogen production using Shimadzu GC-14C gas chromatography. When evaluating the stability properties of the photocatalyst, the system was reacted for five hours, followed by a rigorous outgassing test, which was repeated a total of three times. Use monochromatic filters of different wavelengths to test the apparent quantum efficiency (AQY) of the catalyst, AQY (%) = 2*number of evolved hydrogen molecules /number of incident photons.
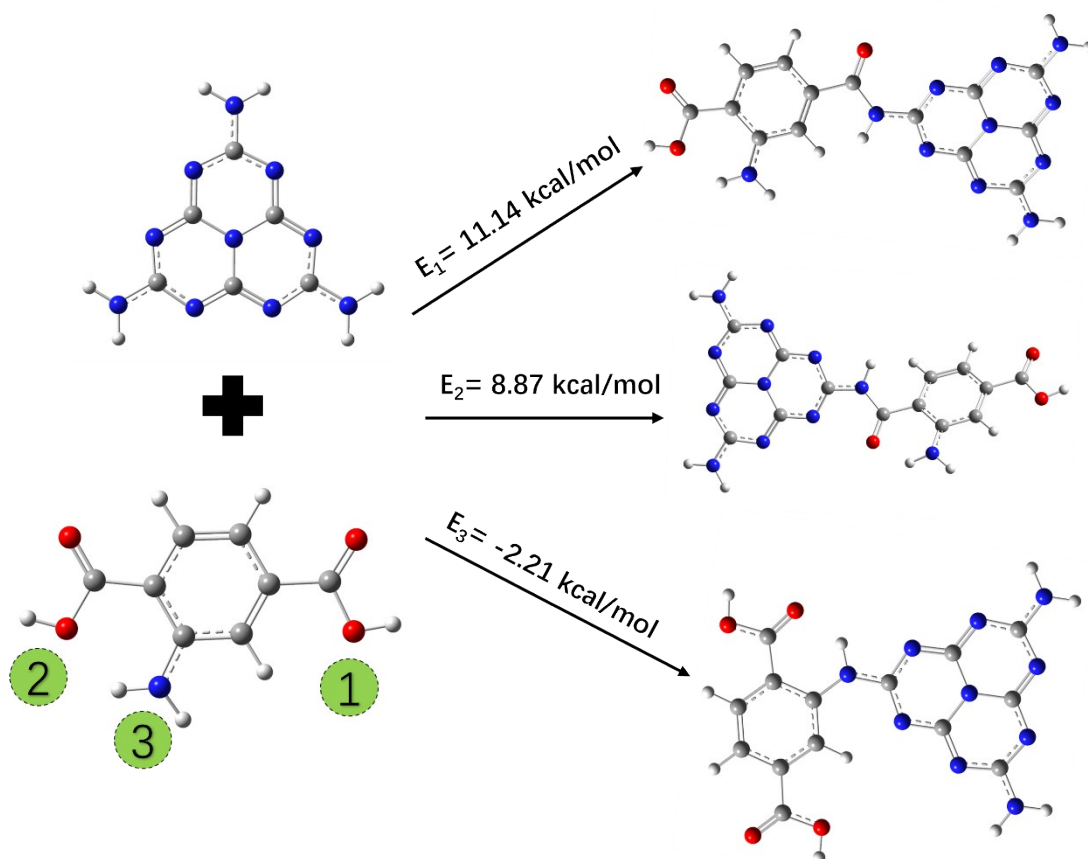
Scheme. S1. Calculated Gibbs Free Energy (ΔG) of melamine and 2-AA. (C, N, O and H are indicated by gray, blue, red and white spheres, respectively.)

The DFT simulation calculated the binding reaction of urea and 2-aminoterephthalic acid (2AA). The melamine is formed via thermal condensation and the release of H_2O molecule under gaseous ammonia condition generated from the pyrolysis of urea. As shown in Scheme S1, there are three possible reactive action sites (noted as 1, 2, 3) in 2AA with the amino group of melamine. The Gibbs Free Energy (ΔG) of melamine and 2AA in the three positions (site 1, 2, 3) is 11.14, 8.87 and -2.21 kcal/mol, respectively. Because of extremely low Gibbs Free Energy ($\Delta G < 0$), the substitution in site 3 is much more favorable the other positions.
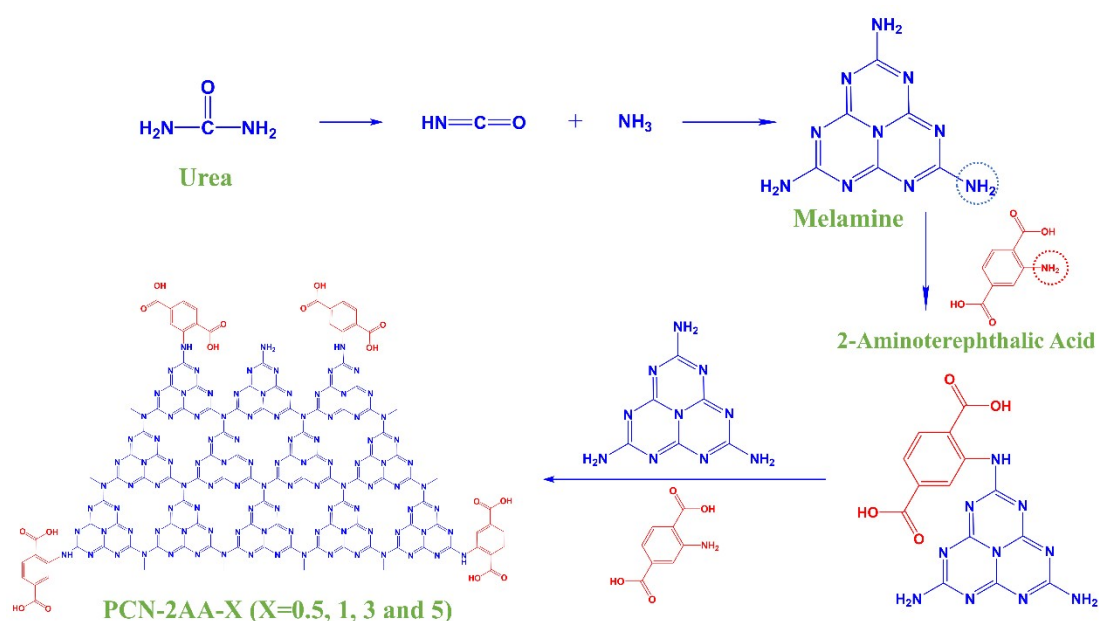
Scheme S2. The Possible Polymerization Reaction Process of PCN-2AA-X (X=0.5, 1, 3 and 5) samples.

Urea is first thermologically polymerized to produce melamine. Then, according to the calculation results in Scheme S1, it can be seen that the amino group on melamine reacts with the amino group on 2AA. According to the amount of 2AA added, a series of PCN-2AA-X (X=0.5, 1, 3 and 5) are finally obtained.
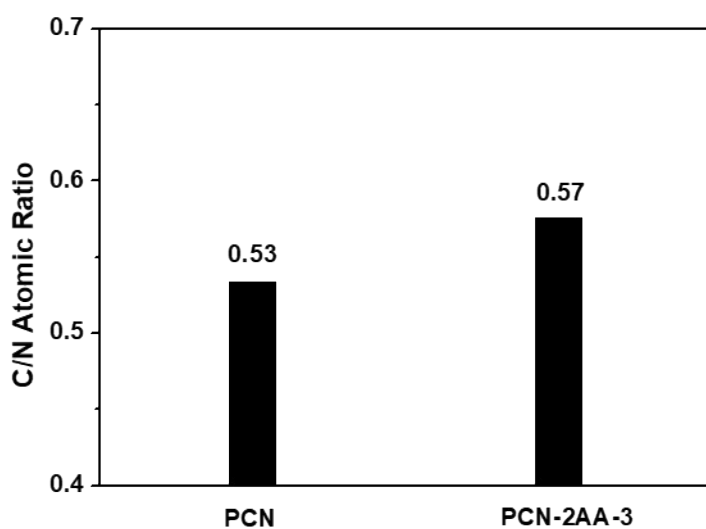
Fig. S1. Elements analysis of PCN and PCN-2AA-3.

Noticeably, the elemental analysis in Fig. S1 show the C/N atomic ratio increases from PCN (0.53) to PCN-2AA-3 (0.57), indicating the possible presence of carbon ring.
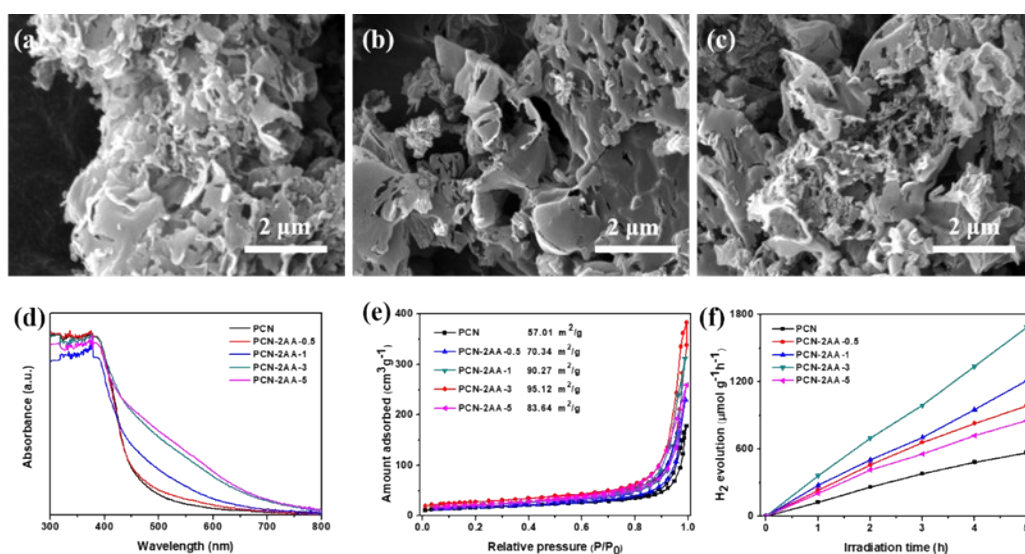

Fig. S2. SEM images of (a) PCN-2AA-0.5, (b) PCN-2AA-1 and (c) PCN-2AA-5, (d) UV−vis DRS spectra, (e) N_2 adsorption-desorption isotherms and (f) photocatalytic hydrogen revolution (HER) plots of PCN, PCN-2AA-0.5, PCN-2AA-1, PCN-2AA-3 and PCN-2AA-5.

As displayed in Fig. S2a-c, the SEM images of PCN-2AA-X samples are similar to that of PCN, which possesses a two-dimensional lamellar structure with uniform mesopores. Fig. R1d displays UV-vis diffuse reflectance spectra (DRS for PCN and a series of PCN-2AA-X samples. The visible absorption region extends from 450 to 650 nm as the 2AA addition increases, indicating excitations by photons with energy lower than that of the intrinsic band-band transition. N_2 adsorption-desorption isotherms at 77 K were performed to investigate the effect of 2AA addition on the specific area of the obtained samples. PCN has a Brunauer-Emmett-Teller (BET) specific surface area of 57.01 m^2/g (Fig. S2e). The BET surface area of PCN-2AA samples first increases from PCN-2AA-0.5 to PCN-2AA-3, then decreases progressively as the 2AA addition increases to 5g (83.64 m^2/g in PCN-2AA-5). The higher BET specific surface area is expected to enhance the number of active sites and inhibiting the recombination of electron-hole, resulting in a higher photoreaction quantum efficacy. As shown in Fig. S2f, PCN-2AA-3 exhibits a maximum hydrogen evolution rate of 1692.1 μmol g^{-1} h^{-1}.
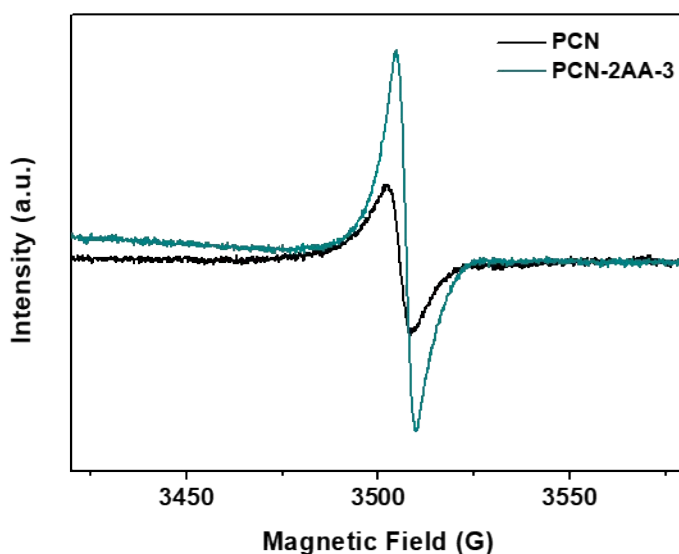

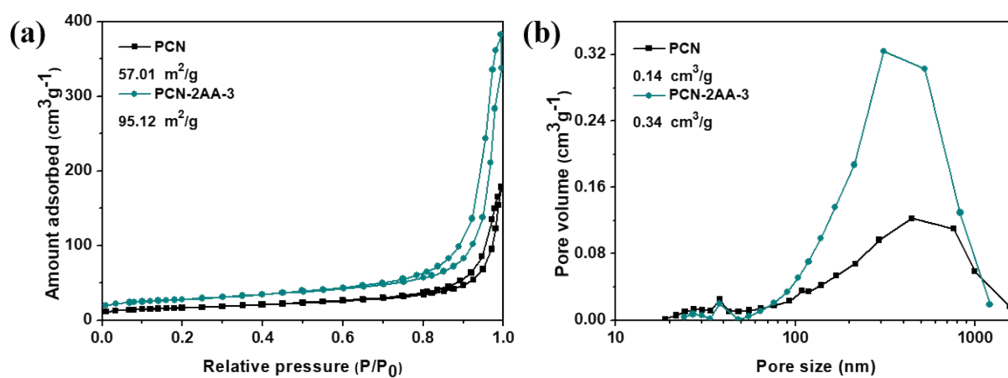**Fig. S3.** ESR spectra of PCN and PCN-2AA-3.

Fig. S4. (a) N_2 Adsorb/desorption isotherms and (b) the pore size distributions of PCN and PCN-2AA-3.
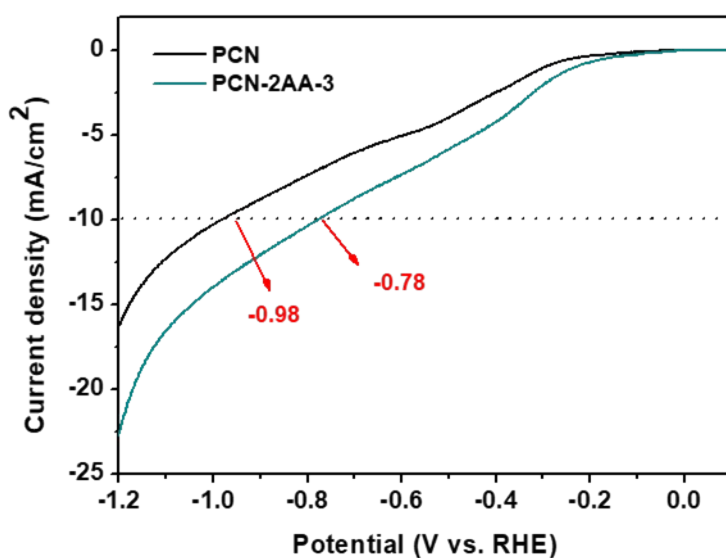

Fig. S5. Polarization curves of PCN and PCN-2AA-3.
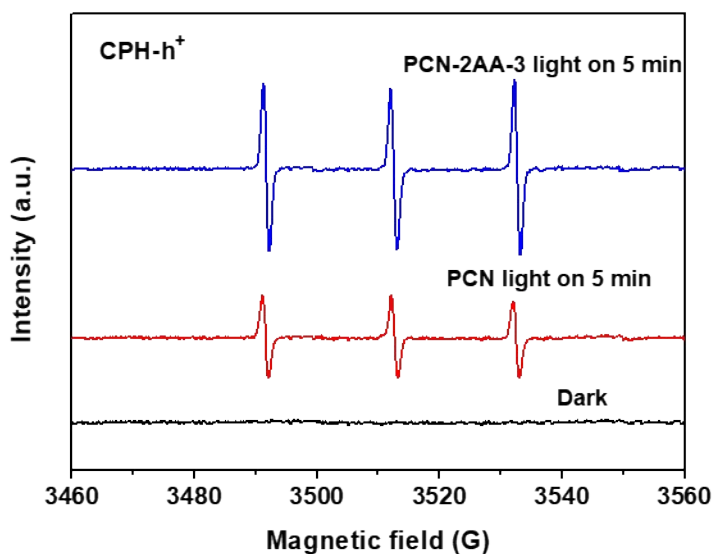
Fig. S6. EPR spectra of CPH-h$^+$ under N$_2$.

Electron paramagnetic resonance (EPR) was conducted using 1-hydroxy-3-carboxy2,2,5,5-tetramethylpyrrolidine (CPH) as capture agents. As shown in Fig. R4, a three-line signal with an intensity ratio of 1:1:1 was observed for both PCN and PCN-2AA-3 under a nitrogen atmosphere, corresponding well with the spectra of the CPH-h$^+$ adduct. This result strongly proves the generation of h$^+$. Furthermore, the signal intensity of h$^+$ for PCN-2AA-3 is much stronger compared with PCN, indicating the generation of more h$^+$ during the H$_2$ generation. The EPR finding demonstrate the presence of h$^+$ throughout the photocatalytic reactions.
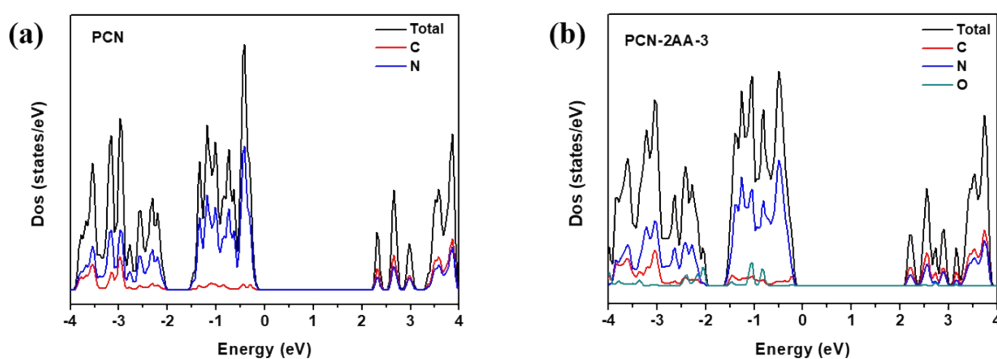

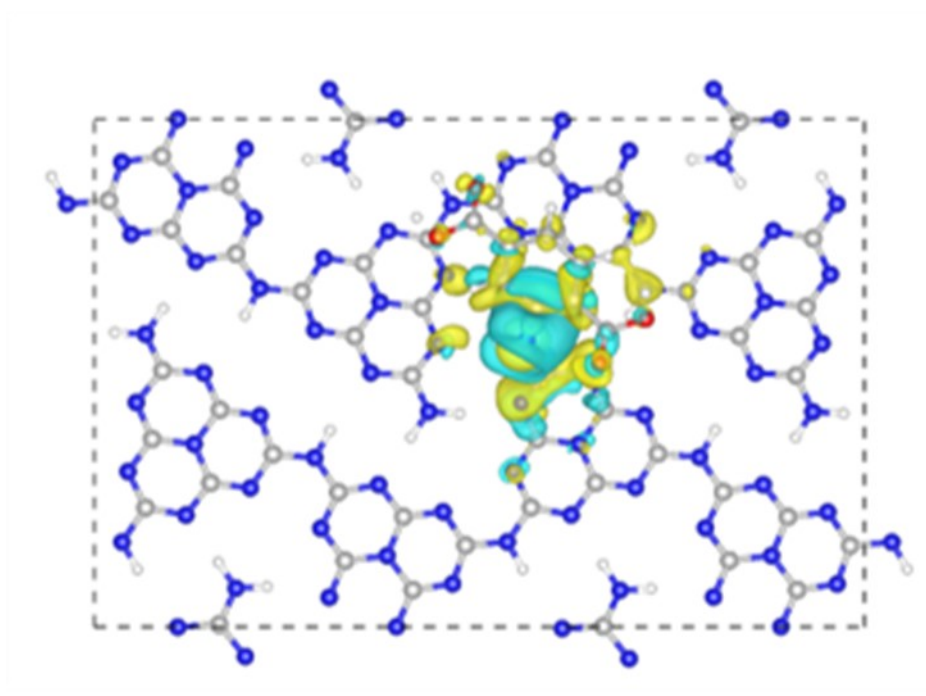**Fig. S7.** Density of states of (a) PCN and (b) PCN-2AA-3.

Fig. S8. The charge density difference of the PCN-2AA-3. Charge accumulation is in yellow and depletion is in light blue.

The difference charge density of PCN-2AA-3 is shown in Fig. S6, a large amounts of net electrons accumulating on the edges of the skeleton connected to the 1,4-dicarboxybenzene, which indicates that the edge induction and delocalization effects of 1,4-dicarboxybenzene are generated in the PCN-2AA-3 framework
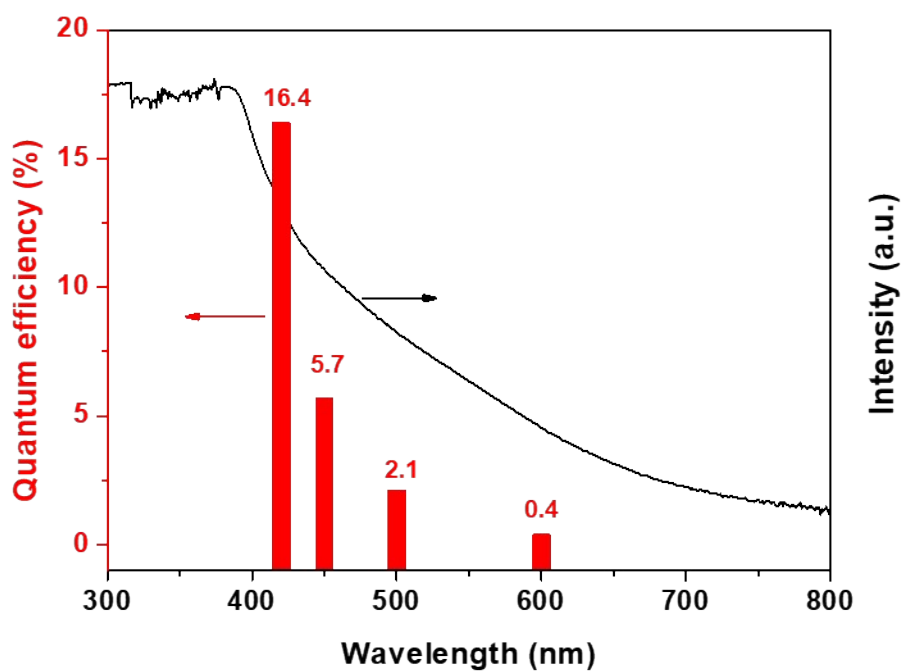
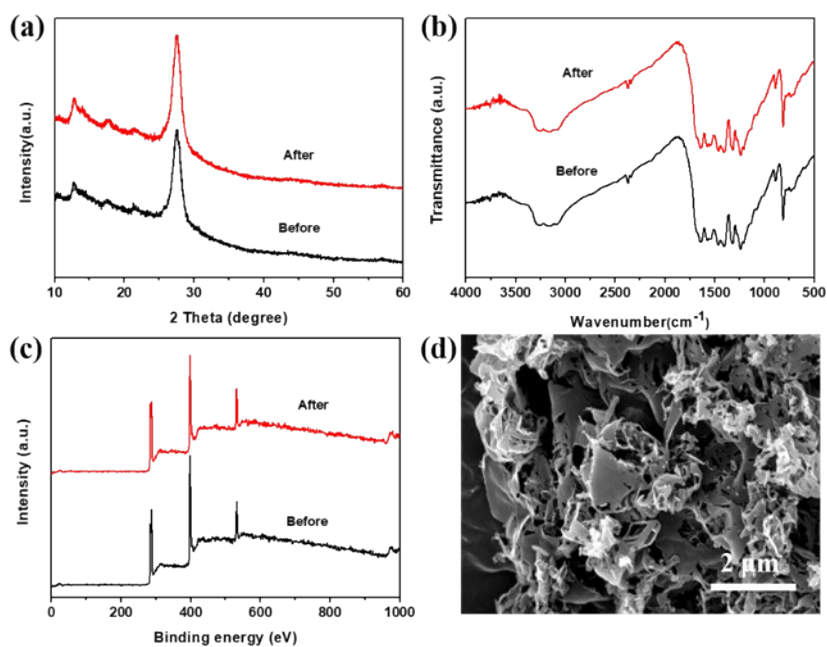**Fig. S9.** AQE values depended on absorption spectrum of PCN-2AA-3.

Fig. S10. (a) XRD patterns, (b) FTIR spectra and (c) XPS survey spectra of the PCN-2AA-3 before and after reaction. (d) SEM image of PCN-2AA-3 after reaction.

Table S1 The fitted fluorescence components of PCN and PCN-2AA3, respectively.

Materials	Decay time/ns		Relative amplitude/%		Average lifetime/ns
	$\tau 1$	$\tau 2$	A1	A2	
PCN	1.02	4.81	0.75	0.29	3.44
PCN-2AA-3	0.84	4.52	0.73	0.30	3.37

Table S2 Summary of the hydrogen evolution reaction activity of PCN based catalysts

Samples	HER rate/ $\mu mol\ h^{-1}\ g^{-1}$	AQE/% (420 nm)	Reference
OCNA-6	662.8	20.42	S1
P-TCN	670	5.68	S2
PTYS CN-2	740	11.8	S3
g-C$_3$N$_4$-4AAP$_{15}$	248.2	24.2	S4
ONLH-600	340	10.3	S5
HTCN-500	890	26.7	S6
MCN-1	60.2	7.8	S7
COCN20	6880	13.2	S8
TCN-MB$_{10}$	2275.6	1.1	S9
PCN-2AA-3	**1692.1**	**16.4**	**This work**

References:

S1. W. Jiang, Q. Ruan, J. Xie, X. Chen, Y. Zhu, J. Tang, Appl. Catal. B: Environ. 2018, 236, 428-435.

S2. S. Guo, Z. Deng, M. Li, B. Jiang, C. Tian, Q. Pan, H. Fu, Angew. Chem. Int. Ed. Engl. 2016, 55, 1830-1834.

S3. N. Tian, K. Xiao, Y. Zhang, X. Lu, L. Ye, P. Gao, T. Ma, H. Huang, Appl. Catal. B: Environ. 2019, 253, 196-205

S4. H. Dong, Y. Zuo, M. Xiao, T. Zhou, S. Cheng, G. Chen, J. Sun, M. Yan, C. Li, ACS Appl. Mater. Interfaces 2021, 13, 56273-56284.

S5. Y. Wang, M. K. Bayazit, S. J. A. Moniz, Q. Ruan, J. Tang, Energ. Environ. Sci. 2017, 10, 1643-1651.

S6. Y. Li, F. Gong, Q. Zhou, X. Feng, J. Fan, Q. Xiang, Appl. Catal. B: Environ. 2020, 268, 118381

S7. Z. Huang, J. Song, L. Pan, Z. Wang, X. Zhang, J. Zou, W. Mi, X. Zhang, L. Wang, Nano Energy 2015, 12, 646-656.

S8. Z. Sun, Y. Tan, X. Shi, B Li, X. Wang, J. Wen, L. Huang, W. Lau, ACS Sustainable Chem. Eng. 2024, 12, 1051-1061.

S9. F Yin, P. Qin, J Xu, S. Cao, Acta Phys. -Chim. Sin. 2023, 39, 2212062.